

PLANETARY IMPACTS: THE EFFECTS OF GRAVITY, SIZE, AND VELOCITY ON THE SCALING OF CRATER GEOMETRY AND THE TRANSITION FROM SIMPLE TO COMPLEX CRATERS  
John D. O'Keefe and Thomas J. Ahrens, Seismological Laboratory 252-21, California Institute of Technology, Pasadena, CA 91125.

To establish scaling relations for the maximum depth of penetration, excavation, and vaporization, as well as the transition diameter from simple to complex crater shapes, we have modelled the impact of projectiles on a planetary surface under wide range of conditions. These include impact velocity ( $U$ ) variations from 12 to 40 km/s, impactor radius ( $a$ ) variations from 5 to  $5 \times 10^6$  m, gravity ( $g$ ) variations from 0 to  $10^9$  cm/s<sup>2</sup>, strength ( $Y$ ) variations from zero to 30 kbar, and vaporization energy ( $E$ ) variations from  $1.8 \times 10^9$  to  $1.8 \times 10^{11}$  erg/g. Planetary deformations and ejecta trajectories are delineated by placing massless tracer particles in planes below the point of impact. We have determined the evolution of the crater depth and diameter and related these to the scaling laws of Holsapple and Schmidt [1]. In addition, we have established scaling relationships for the maximum depth of penetration, excavation and vaporization. We have derived relationships for the scaling of the transition from simple to complex craters and compared these to data on the terrestrial and icy satellites.

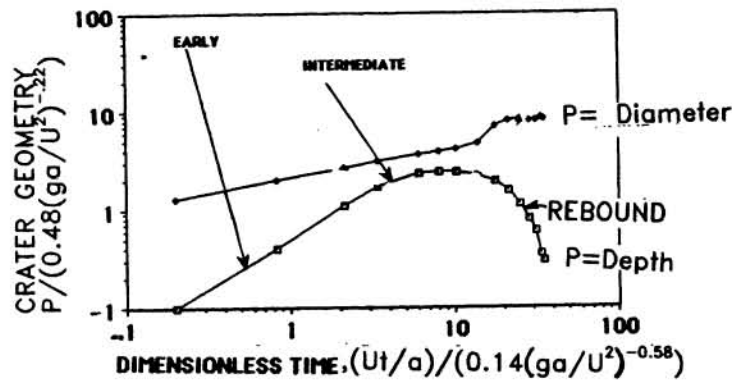
The depth of penetration and the crater diameter and depth as a function of dimensionless time (Figure 1) grow linearly for dimensionless times  $< 5$ . For times greater than 5, the crater grows at a slower but nearly constant rate until it either stops or rebounds. The similitude observed for a wide range of impact parameters agrees with the scaling relationships of Holsapple and Schmidt [1] up to conditions where the concept of a coupling coefficient becomes invalid ( $(ga/U^2) < 10^2$ ) (O'Keefe and Ahrens [2]). The late time motions obey gravity scaling. Shown in Figure 1 is the evolution of the scaled crater depth, and crater diameter as a function of a dimensionless time,  $Ut/a / [0.14 (ga/U^2)^{-0.58}]$ .

At zero and low relative values of strength  $Y/(\rho_0 U^2) \ll 1$  and latent vaporization energy ( $E$ ) levels  $E/U^2 \ll 1$ , the maximum crater depth scales as  $(ga/U^2)^{-0.22}$ . At relatively large values of strength and low gravitational acceleration, the maximum depth scales as  $(Y/\rho_0 U^2)^{-0.19}$ . The transition from simple to complex craters occurs when the gravitational forces due to the size of the transient cavity dominate over the strength driving toroidal flow fields that result in the rebounding of the crater floor. We show that the dynamic transition scales as  $g^{-1}$  for rate independent solids, and scales as  $g^{-0.8}$  for ice and  $g^{-1/3}$  for linearly viscous materials. Shown in Fig. 2 is the data on the transition diameters for the terrestrial planets (Pike [3]) and Jovian and Saturnian satellites (Chapman and McKinnon [4]). The terrestrial planets scale as  $g^{-1}$ , as would be expected for a rate independent rheology. This is the same scaling as Melosh [5] found for his crater collapse model. The icy satellites do not follow the  $g^{-1}$  scaling very closely (Schenk [6]), but are better fit by the rate-dependent scaling derived from the ice strain-rate relationship of Glen.

The mass of impact induced vapor is a function of the impact velocity, porosity, and volatility. For high velocities and/or high surface volatility ( $E/U^2 \ll 1$ ), vaporization can be an important aspect of the crater evolution. An example of a high velocity impact (38 km/s) large scale impact is shown in Figure 3. In this case planetary material is vaporized and expelled from the crater to depths greater than 3 projectile radii. This depth of excavation is slightly greater than for an equivalent energy low velocity impact. However, the maximum depth of penetration of the projectile is greater in the low velocity case. In the high velocity case, material is excavated at all points beneath the point of impact as opposed to the low velocity case where material is excavated only near the crater diameter (O'Keefe and Ahrens, 1987).

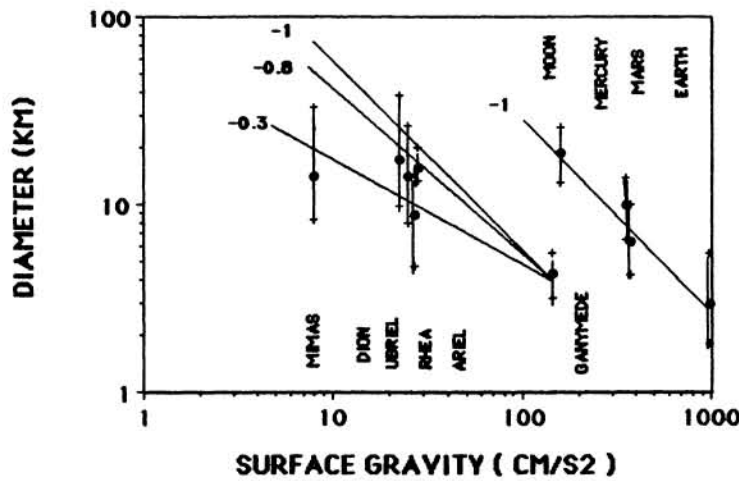
These results imply that the stratigraphy in the crater might be used to discriminate between low and high velocity impacts. Flynn Creek (Roddy, 1968) would be an example of a crater formed by a low velocity (or impedance) impact because the depth of excavated material is greatest near the crater rim. In contrast, the Ries crater because of its maximum depth of excavation occurs in the center and is an example of a crater that could be interpreted as being formed by a high velocity impact.

References: [1] Holsapple, K.A. and R.M. Schmidt (1987), *J. Geophys. Res.*, **92**, 6350-6376. [2] O'Keefe, J.D. and T.J. Ahrens (1987), *LPSC XVIII*, 745. [3] Pike, R.J. (1988), *Mercury* (eds. C. Chapman, F. Vilas, and M. Matthews) Univ. of Ariz. Press, Tucson, 165-273. [4] Chapman, C. and W.B. McKinnon (1986), in *Satellites*, Univ. of Arizona Press, 492. [5] Melosh, H.J. (1982), *J. Geophys. Res.*, **87**, 1880. [6] Schenk, P.M. (1988), *Abstract, Lunar and Planetary Science*, **XIX**, 1027-1028.



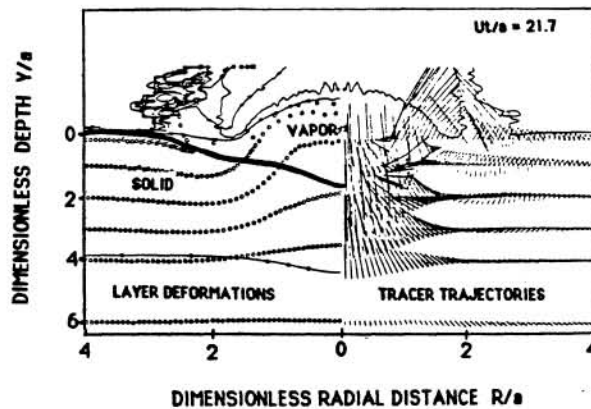
TJA89014SFD

Fig. 1. Scaled crater geometry parameter, P=depth (d) and diameter (D) normalized to projectile radius (a) as a function of dimensionless time.



TJA89015SFD

Fig. 2. Simple to complex transition diameter for icy satellites (Schenk, 1988) and terrestrial planets (Pike, 1988). Slope of -1 is for rate independent solids, -0.8 for ice using Glen's law and -0.3 for linearly viscous materials.



TJA89016SFD

Fig. 3. Cratering flow field at a dimensionless time of 22.7 for 50 km radius silicate projectile impacting earth at 38 km/sec. Left side shows deflection of horizontal tracer particles and density contours ( $g/cm^3$ ). Right side shows trajectory of tracer particles.